1
Introduction

Microwave remote sensing infers the physical parameters from satellite radiometers that operate at wavelengths ranging from millimeters to centimeters (1.0 mm to 20.0 cm). The microwave radiometers are generally of two types: imagers that have channels in the window regions of the spectrum to monitor surface, cloud, and precipitation; and sounders that have channels in opaque spectral regions to profile atmospheric temperature and water vapor under all weather conditions. All the current and planned instruments are flown aboard low Earth-orbiting satellites. The vantage point of the geosynchronous orbit would be valuable for obtaining the synoptic and continuous views of the atmosphere provided by optical and infrared sensors.

This chapter introduces some fundamental parameters used in microwave remote sensing.

1.1
A Microwave Radiometer System

A typical microwave radiometer uses the so-called heterodyne principle applied at radio frequencies. A heterodyne receiver is one in which the received signal, called the radio frequency (RF) signal, is translated to a different and usually lower frequency (the intermediate-frequency (IF)) signal before it is detected. The simplest heterodyne radiometer is shown in Figure 1.1. It is an example of a total-power radiometer and illustrates the features common to most microwave radiometers. As a signal at some frequency is incident upon the antenna of the radiometer, it couples the RF signal into a transmission line (a waveguide, for example), the function of which is to carry the RF signal to and from the various elements of the circuit. In the example, this signal is introduced directly into a mixer, which is a nonlinear circuit element in which the RF signal is combined with a constant-frequency signal produced at the output of this element because of its nonlinearity. These products include a signal whose frequency is the difference between the RF and local oscillator (LO) frequencies. This signal has the important property that its power is proportional to the power in the RF signal under the condition that the

Passive Microwave Remote Sensing of the Earth: For Meteorological Applications, First Edition. Fuzhong Weng.

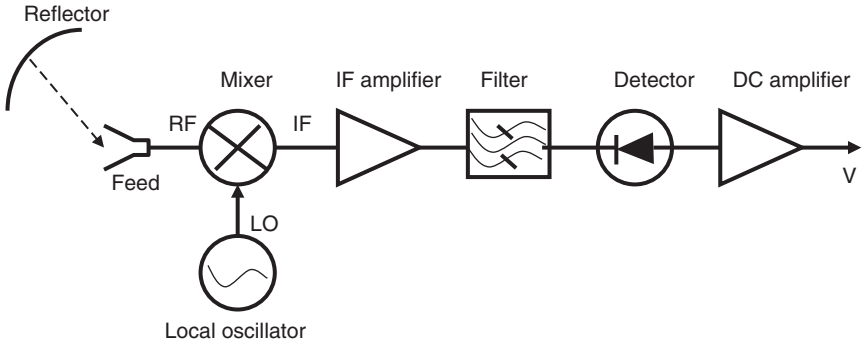

Figure 1.1 Schematic of a microwave radiometer with a circuit that produces an output voltage proportional to the received signal power.

latter is much weaker than the LO signal. It is then filtered to exclude the unwanted products of the mixing and amplified to produce the IF output signal.

The total-power radiometer produces an output voltage V, which is a polynomial function of the input current I:

$$V = a_1 I + a_2 I^2 + a_3 I^3 + a_4 I^4. \tag{1.1}$$

For a perfect square-law detector, the last two terms vanish. After integration over time and considering the current as a sinusoidal function of time, the average voltage is a function of the current squared:

$$\overline{V} = (a_2 + 3a_4 I^2) I^2. \tag{1.2}$$

Using the Nyquist theorem, this current squared is related to the total power input to the IF system, which is the sum of the thermal radiation $R(T_A)$ from the measurement target and the noise $R(T_n)$:

$$I^2 = KBG[R(T_A) + R(T_N)], \tag{1.3}$$

where T_A, G, B, and T_N are the temperature of the measurement target, amplifier gain, bandwidth, and noise temperature, respectively, and K is the Boltzmann constant.

It is seen from Eq. (1.3) that for the total-power radiometer, the amplifier gain and noise affect the mean voltage. In order to reduce the effect of the internal amplifier noise on the output stability, Dicke [1] introduced a radiometer circuit that can eliminate the noise term through differentiating the signals from the measuring target and an internal load with a known temperature during one integration cycle. The Dicke radiometer was a great invention and was used to measure

the low power levels associated with thermal microwave radiation. The use of an internal noise diode injecting noise at a known temperature into the receiver can also reduce the effects of the gain instability and internal noise on the output of the total-power radiometer.

Combining Eqs. (1.2) and (1.3) results in

$$V = b_0 + b_1 R(T_A)[1 + \mu R(T_A)], \tag{1.4a}$$

where μ is the nonlinear parameter, and b_0 and b_1 are the parameters that can be directly determined from two-point calibration. They are mathematically expressed as

$$b_0 = [a_2 + 3a_4 KBR(T)]KBGR(T), \tag{1.4b}$$

$$b_1 = [a_2 + 6a_4 KBR(T)]BG, \tag{1.4c}$$

$$\mu = 3a_4 \frac{KBG}{a_2}. \tag{1.4d}$$

1.2 Blackbody Emission

A blackbody is an object that absorbs light at a certain wavelength and also emits radiation at the same wavelength. The total amount of energy radiated by a blackbody can be described through Planck's law in a special function. The function is valid for electromagnetic radiation pervading any medium, regardless of its constitution, that is in thermodynamic equilibrium at a definite temperature. If the medium is homogeneous and isotropic, then the radiation is homogeneous, isotropic, unpolarized, and incoherent. The law is named after Max Planck, who originally proposed it in 1900. It is a pioneer result of modern physics and quantum theory. For a wave number υ, Planckian radiation or spectral radiance (in unit: W/m^2/sr/cm) is expressed as

$$B_\upsilon(T) = \frac{2hc^2\upsilon^3}{\exp\left(\frac{hc\upsilon}{kT}\right) - 1} \equiv \frac{C_1\upsilon^3}{\exp\left(\frac{C_2\upsilon}{T}\right) - 1}, \tag{1.5}$$

where the Planck constant $h = 6.626 \times 10^{-34}$ J s; the Boltzmann constant $k = 1.381 \times 10^{-23}$ J/K; c is the speed of light, $C_1 = 2hc^2 = 1.1909 \times 10^{-8}$ W/m^2/sr/cm^3, and $C_2 = \frac{hc}{k} = 1.438786$ cm/K.

It should be pointed out that the Planck function can be expressed in terms of wavelength or frequency, but the resultant unit is different. When the energy is integrated within a wavelength, wave number, or frequency domain, the unit for the radiance should be all the same (W/m^2/sr). For example, in a

frequency domain f,

$$B_f(T) = \frac{2hf^3}{c^2} \frac{1}{\exp\left(\frac{hf}{kT}\right) - 1}, \tag{1.6}$$

which represents the energy in $\mathrm{W/m^2/sr/Hz}$. Alternatively, it can be written in terms of the wavelength λ, as

$$B_\lambda(T) = \frac{2hc^2}{\lambda^5} \frac{1}{\exp\left(\frac{hc}{\lambda kT}\right) - 1}, \tag{1.7}$$

which represents the energy in $\mathrm{W/m^2/sr/cm}$.

An integration for radiance within a spectrum can be derived using any function from Eqs. (1.5)–(1.7) with a relationship to the frequency, wavelength, and wave number for changing the limits in the integration. For instance, we can use Eq. (1.6) with $f = c\upsilon$ and $f = \frac{c}{\lambda}$

$$I = \int_{f_1}^{f_2} B_f(T)\mathrm{d}f = \int_{\upsilon_1}^{\upsilon_2} B_\upsilon(T)\mathrm{d}\upsilon = \int_{\lambda_1}^{\lambda_2} B_\lambda(T)\mathrm{d}\lambda. \tag{1.8}$$

Thus, we can also understand the equivalence of the Planck function expressed as Eqs. (1.5)–(1.7), which are interchangeable through

$$B_\upsilon(T) \equiv B_f(T)c, \tag{1.9}$$

$$B_\lambda(T) \equiv B_f(T)\frac{c^2}{\lambda^2}, \tag{1.10}$$

$$B_\upsilon(T) \equiv B_\lambda(T)\lambda^2. \tag{1.11}$$

1.3 Linearized Planck Function

Assuming $\frac{C_2\nu}{T} \ll 1$, the exponential term in the Planck function can be expressed as a Taylor series:

$$\exp\left(\frac{C_2\upsilon}{T}\right) = 1 + \frac{C_2\upsilon}{T} + \frac{1}{2}\left(\frac{C_2\upsilon}{T}\right)^2 + \cdots + \frac{1}{n!}\left(\frac{C_2\upsilon}{T}\right)^n + \cdots. \tag{1.12}$$

Substituting the first-order approximation of the given Taylor expansion into Eq. (1.5), one obtains the following linear relationship between the blackbody temperature (T) and radiance $B_\upsilon(T)$, which is also referred to as the Rayleigh–Jeans (RJ) approximation:

$$B_\upsilon^{RJ}(T) = \frac{C_1\upsilon^2}{C_2}T. \tag{1.13}$$

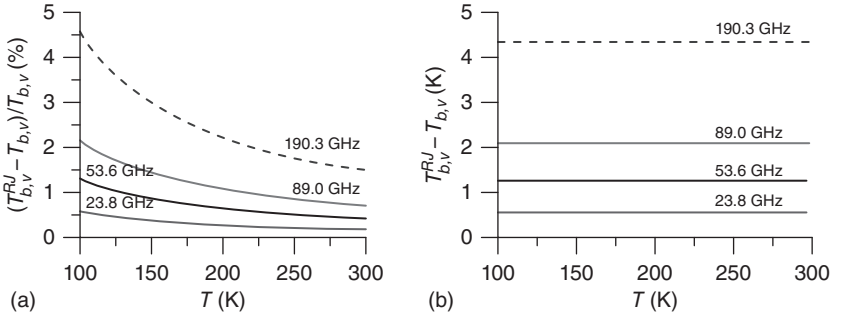

Figure 1.2 (a) Relative and (b) absolute variations of the brightness temperature with blackbody temperature varying from 100 to 300 K at frequencies 23.8, 53.6, 89.0, and 190.3 GHz. (Weng and Zou 2013 [2]. Reproduced with permission of Optical Society of America.)

The accuracy of the radiance calculated from Eq. (1.5) and the linear approximation Eq. (1.13) varies with the frequency and temperature. Figure 1.2 shows the relative accuracy of the first-order approximation of the Planck function $(B_\nu^{RJ} - B_\nu)/B_\nu$ with respect to temperature at four arbitrarily selected frequencies of 23.8, 53.6, 89.0, and 190.3 GHz. At a fixed temperature, the higher the frequency, the larger the error. Alternatively, at a fixed frequency, the lower the temperature, the larger the error. At a high frequency near 190.3 GHz, there is a 4.5% error in radiance. The error decreases rapidly with an increase in temperature. More analyses of the RJ approximation can be found in Weng and Zou [2].

1.4 Stokes Vector and Its Transformation

When an electromagnetic wave propagates in space, both its electric and magnetic fields are expressed as vectors, and they travel through space by exciting the field of each other. As a result, the radiation field is a Stokes vector with four elements which are related to the amplitudes of the electric field in the form

$$\mathbf{I} = (I, Q, U, V) \tag{1.14a}$$

or

$$\mathbf{I} = (I_\parallel, I_\perp, U, V) \tag{1.14b}$$

where

$$I = \langle E_\parallel E_\parallel^* \rangle + \langle E_\perp E_\perp^* \rangle, \tag{1.15a}$$

$$Q = \langle E_\parallel E_\parallel^* \rangle - \langle E_\perp E_\perp^* \rangle, \tag{1.15b}$$

$$I_\parallel = \langle E_\parallel E_\parallel^* \rangle, \tag{1.15c}$$

$$I_{\perp} = \langle E_{\perp} E_{\perp}^{*} \rangle, \tag{1.15d}$$

$$U = \langle E_{\parallel} E_{\perp}^{*} \rangle + \langle E_{\perp} E_{\parallel}^{*} \rangle, \tag{1.15e}$$

$$V = i\langle E_{\parallel} E_{\perp}^{*} \rangle - \langle E_{\perp} E_{\parallel}^{*} \rangle, \tag{1.15f}$$

where $E_{\parallel}$ and $E_{\perp}$ are the horizontal and vertical components of the electric field, respectively, the star $(*)$ denotes the conjugate of a complex value, and the angular brackets indicate the time average over an interval longer than the oscillation period of the electric field.

The component expressed by Eq. (1.15a) also represents the total energy from the electromagnetic field and thus is also referred to as the radiation intensity. In the microwave remote sensing field, the subscripts $\parallel$ and $\perp$ are often replaced with h and v in the first two Stokes components. Thus, in this textbook, we use the following notations for the Stokes brightness temperature components:

$$\mathbf{T}_b = (T_b^h, T_b^v, T_b^3, T_b^4), \tag{1.16}$$

where the superscripts (3, 4) are used in the brightness temperature components in Eq. (1.16) to replace the third and fourth Stokes components in Eqs. (1.15c) and (1.15d) for avoiding the repetition of the superscripts used in the first two components. The four brightness temperature components are related to the Stokes parameters in Eq. (1.15) through the Planck function.

The law of transformation of the Stokes parameters for a rotation of the axes through an angle θ is derived in two forms. For the Stokes parameters expressed in Eq. (1.14a), the transformation matrix [3] is given as

$$\mathbf{L}_i = \begin{pmatrix} 1 & 0 & 0 & 0 \\ 0 & \cos 2i & -\sin 2i & 0 \\ 0 & \sin 2i & \cos 2i & 0 \\ 0 & 0 & 0 & 1 \end{pmatrix}. \tag{1.17a}$$

Alternatively, it can be written as

$$\mathbf{L}_i = \begin{pmatrix} \cos^2 i & \sin^2 i & \frac{1}{2}\sin 2i & 0 \\ \sin^2 i & \cos^2 i & -\frac{1}{2}\sin 2i & 0 \\ -\sin 2i & \sin 2i & \cos 2i & 0 \\ 0 & 0 & 0 & 1 \end{pmatrix}, \tag{1.17b}$$

when the Stokes parameters in Eq. (1.14b) are used [4].

Equation (1.17b) is often used in microwave remote-sensing applications. For a Stokes vector having zero third and fourth components in one coordinate

system, its rotation to other coordinate systems may result in nonzero third and fourth components. The third and fourth Stokes components can also contribute to the first and second components through a coordinate transformation. For a microwave scanning radiometer, Eq. (1.17b) is applied for converting the brightness temperature components at the local coordinate to those at a scan angle θ with respect to the nadir position such that

$$T_b^{Qh} = T_b^h \cos^2\theta + T_b^v \sin^2\theta - T_b^3 \frac{1}{2} \sin 2\theta, \tag{1.18a}$$

and

$$T_b^{Qv} = T_b^h \sin^2\theta + T_b^v \cos^2\theta + T_b^3 \frac{1}{2} \sin 2\theta, \tag{1.18b}$$

respectively, where the subscripts on the left-hand side of Eq. (1.18) denote the first two components of the Stokes vector after the coordinate transformation. The third terms on the right-hand side are normally neglected in microwave calibration [5]. However, for the window channels over the polarized surfaces, the third term could be significant, and further studies are needed to quantify the magnitude in microwave instrument calibration.

1.5 Microwave Spectrum

In microwave remote sensing, the spectrum ranges from centimeter wavelength to millimeter wavelength. The microwave spectrum is usually defined as electromagnetic energy ranging from ~1 to 200 GHz in frequency, but older usage includes lower frequencies. Most common applications are within the 1–60 GHz range. Microwave frequency bands, as defined by the Radio Society of Great Britain (RSGB), are shown in Table 1.1. L-band technology is used for remote sensing of soil moisture. C- and X-bands are more utilized for remote sensing of ocean properties such as sea-surface temperature and wind vector. K-band is more sensitive to atmospheric clouds, water vapor, and precipitation. V-band is explored for probing the atmospheric temperature profile. W- and G-bands are used for remote sensing of ice cloud and of atmospheric moisture profile. F-band is also considered as an alternative for atmospheric temperature sounding at a high spatial resolution.

The microwave bands used for meteorological applications are always protected from other emission sources operating at the same frequencies for commercial and military applications. The growing competition may result in strong interferences of the weather microwave instruments with active sources. It is important to develop some techniques to detect the RF interferences on microwave instruments [6, 7].

Table 1.1 Microwave frequency bands used for Earth environmental and atmospheric remote sensing.

Band	Frequency range (GHz)	Major remote sensing applications	RFI sources
L	1–2	Soil moisture content, water salinity	Radar, cell phone, garage door
S	2–4	No applications in passive microwave remote sensing	Radar
C	4–8	Sea surface temperature, soil moisture	Radar, speed monitor
X	8–12	Sea surface wind, sea surface temperature	Direct TV
Ku	12–18	No applications in passive microwave remote sensing	
K	18–26.5	Precipitation, atmospheric water vapor, cloud water, sea surface wind	Direct TV
Ka	26.5–40	Precipitation, water vapor, cloud water, sea surface wind	
Q	30–50	No applications in passive microwave remote sensing	
U	40–60	No applications in passive microwave remote sensing	
V	50–75	Atmospheric temperature profile	
E	60–90	No applications in passive microwave remote sensing	
W	75–110	Precipitation over land, cloud water, and cloud ice	
F	90–140	Atmospheric temperature and moisture profile	
D	110–170	No applications in passive microwave remote sensing	
G	150–190	Atmospheric moisture profile	

1.6 Spectral Response Function

For a typical instrument, the radiance received at a central wavelength corresponds to the radiation within a spectral band and can be expressed as

$$I_f = \int_{f-\Delta f}^{f+\Delta f} B_x(x)S(x)\mathrm{d}x, \tag{1.19}$$

where f is the instrument central frequency, and $2\Delta f$ is the instrument bandwidth, which is determined by the 3-dB window in $S(x)$.

In the past, the instrument spectral response function was not well characterized for many microwave sensors. Thus, it is often assumed as a boxcar function or a Gaussian distribution function. As shown in Figure 1.3, the boxcar, $S(x)$, for the Advanced Technology Microwave Sounder (ATMS) at some channels could be significantly different from the one measured from the laboratory data.

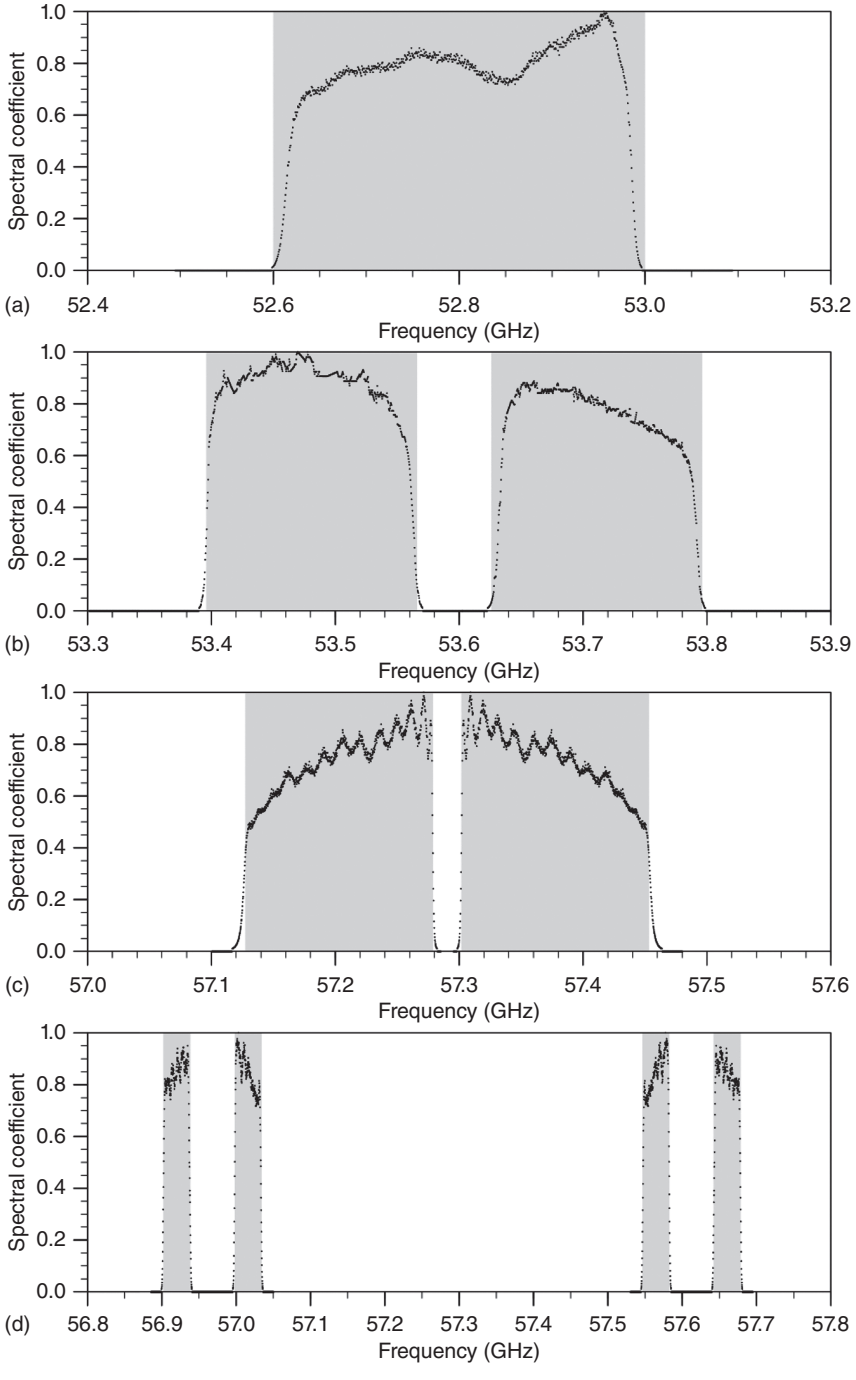

Figure 1.3 Laboratory-measured SRF used in line-by-line model after −20 dB truncation (black line) and the boxcar SRF used in CRTM (shading) for ATMS channel (a) 5, (b) 6, (c) 10, and (d) 12. (Replotted from Zou *et al.* 2014 [8].)

The radiance differences between a boxcar spectral response function (SRF) and the laboratory SRF were recently studied and could be significant for some instruments [8].

1.7 Microwave Antenna Gain and Distribution Function

A microwave radiometer system requires an antenna to collect the radiative energy from the Earth and other targets. The antenna gain or efficiency is determined by its power distribution function, as shown in Figure 1.4. An antenna having a higher gain tends to have a main lobe or beam with a larger power value. The secondary and third peaks are called the side lobes. For an antenna subsystem, the magnitude of the side lobes depends on both the frequency and the antenna size. In general, the higher the frequency and the larger the antenna size, the narrower the main beam and the smaller the side-lobe effect. The antenna pattern is often shown at a decibel scale through normalizing the measured intensity in each direction by the sum of the co- and cross-polarized radiations.

The antenna's main beam width θ is defined through the half-power points in the antenna power function. Based on the normalized antenna pattern, the main beam efficiency is integrated with the antenna angles within 2.5 times the beam width, as follows:

$$\eta_m^{pp} = \int_{\Omega_m} G^{pp} \mathrm{d}\Omega \Big/ \int_{\Omega} (G^{pp} + G^{qp}) \mathrm{d}\Omega. \tag{1.20}$$

The antenna side-lobe efficiency is similarly derived as

$$\eta_s^{pp} = \int_{\Omega_s} G^{pp} \mathrm{d}\Omega \Big/ \int_{\Omega} (G^{pp} + G^{qp}) \mathrm{d}\Omega, \tag{1.21}$$

where the superscripts pp and qp stand for either v or h polarization state; G^{pp} and G^{qp} are the normalized antenna gains in the far field (i.e., Earth and cold space)

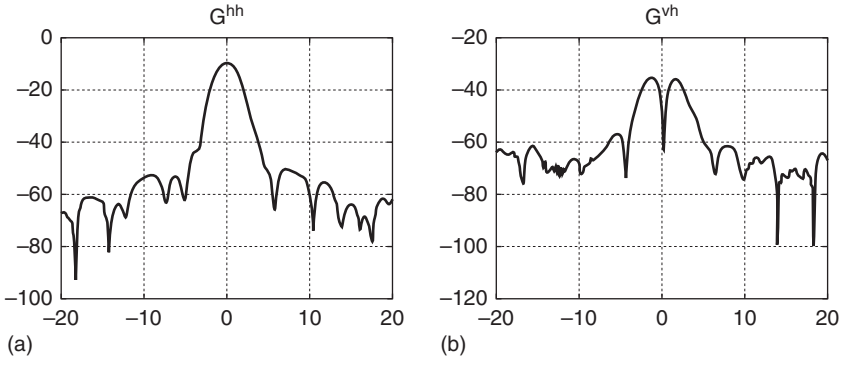

Figure 1.4 ATMS normalized antenna pattern for channel 1 at (a) co-polarization and (b) cross-polarization. (Replotted from Weng *et al.* 2013 [9].)

for co- and cross-polarization, respectively; and Ω_m and Ω_s are the solid angles corresponding to the antenna's main beam and side lobes, respectively. Normally, the side-lobe efficiency is derived according to the portions that intercept the energy from the unwanted targets [9].

1.8 Microwave Instrument Scan Geometry

Similar to a radar system, a satellite microwave instrument also requires an antenna subsystem to scan and collect the energy within its field of view (FOV). Currently, two scanning modes (stepwise or continuous) are deployed in space for cross-track scanning instruments, with the two specific examples illustrated here. The most important parameters are listed in Table 1.2.

The Advanced Microwave Sounding Unit (AMSU-A) is a stepwise scanning instrument. It has a scan angle of ±48.33° with respect to the nadir direction. The instantaneous field of view (IFOV) of each channel is ~57.6 mrad (3.3°),

Table 1.2 Parameters from stepwise and continuous scanning microwave radiometer systems.

Parameter	Symbol	Definition	AMSU (1–15)	ATMS (3–16)
Instantaneous field of view	IFOV	Angular range corresponding to 3-dB points in antenna gain distribution function	3.3°	2.1°
Effective field of view	EFOV	Angular range during which the antenna collects the signal to produce a mean signal	3.3°	2.3°
Angular swath width	θ_m	The maximum value of the instrument scan angle	±48.33°	±52.75°
Number of field of views	N_s	The number of scan-angle positions across each scan	30	96
Scan cycle	T	Total time for antenna viewing Earth, calibration target, then returning to its original position	8 s	8/3 s
Earth view time	T_c	The time of antenna viewing the Earth scene	6 s	1.73 s
Sample time	ΔT	The time for the two consecutive samples made within a scan line	200 ms	18 ms
Sampling angle	θ_s	The time for the two consecutive samples made within a scan line	3.3°	1.1°
Integration time	Δt	The time during which the antenna collects the signal to produce a mean signal	158 ms	17.6 ms
Earth view scan rate	R	The scan rate with which the antenna views the earth scene. These parameters are often related with each other	n/a	61.6 °/s

leading to a circular IFVO size close to 47.63 km at nadir and a swath width of ±1026.31 km for a nominal satellite altitude of 833 km. Its sampling time is 200.0 ms, with 160 ms for integration and 40 ms for stepping to the next scan position. The sampling angular interval is close to 58.18 mrad (3.3333°). The distance between two consecutive scans is ~52.69 km. On each scan line, there are 30 Earth views. Each scan takes 8.0 s to complete.

Microwave instruments can continuously scan across the track. For ATMS, channels 3–16 have a beam width of 2.2°, which is smaller than that of the AMSU-A channels 1–15. However, the beam width for ATMS surface channels 1 and 2 is 5.2°, which is much larger than that of the corresponding AMSU channels 1 and 2. Six of the seven ATMS channels above 60 GHz, channels 17–22, have a beam width of 1.1°, which is the same as that of the water vapor sounding channels of AMSU-A and the microwave humidity sounder (MHS).

The aforementioned differences of the beam width between ATMS and AMSU channels, along with the difference in the satellite altitudes between Suomi NPP (National Polar-orbiting Partnership) (824 km) and its predecessors such as NOAA-19 (870 km), result in significant differences in FOV sizes between ATMS and AMSU. At ATMS channels 1 and 2, its single FOV is ~1.6 times the AMSU FOV in diameter, which is mostly determined by the beam width differences between the two instruments. There is no overlap between the neighboring FOVs and between the neighboring scan lines of AMSU, but significant overlaps occur for ATMS FOVs and scan lines of channels 1 and 2 (Figure 1.5). For example, the FOV48 has overlaps with the neighboring four FOVs and four scan lines.

A single AMSU FOV for channels 3–15 is about 1.5 times larger than that of ATMS channels 3–16. At these channels, a single ATMS FOV overlaps with its surrounding four FOVs. The differences in FOVs for water vapor channels between ATMS and AMSU are rather small. There is a small difference in the integration time between ATMS (18 ms) and MHS (19 ms).

The oversampling features of ATMS allow the estimation of brightness temperatures at resolutions higher or lower than the raw ATMS data resolution. However,

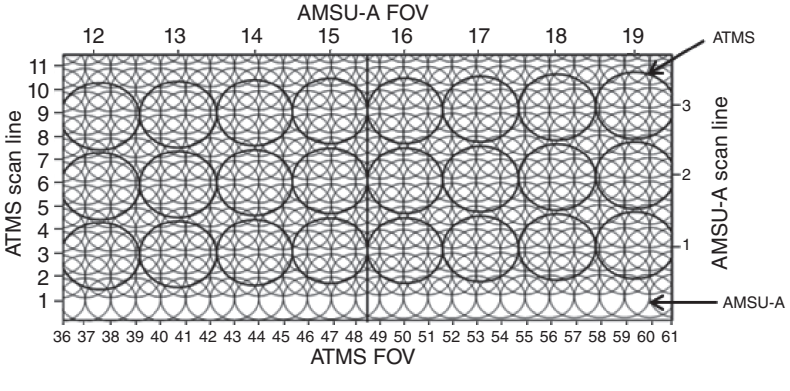

Figure 1.5 Comparison of FOVs from stepwise and continuous scanning microwave radiometers (AMSU-A vs ATMS).

an optimal balance between the desirable resolution and the resulting data noise must be taken into consideration when developing such an estimate for investigating specific weather systems.

1.9 Microwave Data Records and Their Terminology

A microwave radiometer measures the energy averaged within its FOV. Its antenna brightness temperature is defined as

$$T_a^p = \int_{\Omega_{me}} (G^{pp} T_b^p + G^{qp} T_b^q) \mathrm{d}\Omega + \int_{\Omega_{se}} (G^{pp} T_b^p + G^{qp} T_b^q) \mathrm{d}\Omega + \int_{\Omega_{sc}} (G^{pp} T_b^p + G^{qp} T_b^q) \mathrm{d}\Omega + \int_{\Omega_{ss}} (G^{pp} T_b^p + G^{qp} T_b^q) \mathrm{d}\Omega, \tag{1.22}$$

where T_b^p is the brightness temperature at the polarization state of p. Note that T_b^p has a spatial distribution covering the Earth, cold space, and the spacecraft. Ω_{se} and Ω_{ss} are the solid angles of the side lobes facing the cold space and the satellite platform, respectively. The solid angle Ω_{me} corresponds to 2.5 times the main beam width. The first term in Eq. (1.22) is the Earth radiation entering into the receiver system through the main beam; the second term is the Earth radiation through the side lobes that are out of the main beam but within the Earth view sector, the third term is the cold space radiation through the side lobes, and the fourth term is the radiation scattered and emitted from the satellite platform to the receiver. Equation (1.22) can also be expressed in terms of the antenna efficiency associated with each term as

$$T_a^p = \eta_{me}^{pp} T_b^p + \eta_{me}^{qp} T_b^q + \eta_{se}^{pp} T_{b,se}^q + \eta_{se}^{qp} T_{b,se}^q + \eta_{sc}^{pp} T_{b,sc}^q + \eta_{sc}^{qp} T_{b,sc}^q + \eta_{ss}^{pp} T_{b,ss}^p + \eta_{ss}^{qp} T_{b,ss}^q. \tag{1.23}$$

The sensor brightness temperature is derived from Eq. (1.23) by correcting the effects of the cross-polarization and side-lobe contributions from the Earth, cold space, and spacecraft on the antenna brightness temperature:

$$T_b^p = \frac{1}{\eta_{me}^{pp}} (T_a^p - \eta_{me}^{qp} T_b^q - \eta_{se}^{pp} T_{b,se}^q - \eta_{se}^{qp} T_{b,se}^q - \eta_{sc}^{pp} T_{b,sc}^p - \eta_{sc}^{qp} T_{b,sc}^q - \eta_{ss}^{pp} T_{b,ss}^p - \eta_{ss}^{qp} T_{b,ss}^q). \tag{1.24}$$

Determination of the contributions from cross-polarization and side lobes requires both accurate antenna gain efficiencies and brightness temperatures within various sectors viewed by the antenna.